

Orbital-selective correlations for topology in $\text{FeSe}_x\text{Te}_{1-x}$

Zhiguang Liao,¹ Rong Yu,^{1,2,*} Jian-Xin Zhu,^{3,†} and Qimiao Si^{4,‡}

¹*Department of Physics and Beijing Key Laboratory of Opto-electronic Functional Materials & Micro-nano Devices, Renmin University of China, Beijing 100872, China*

²*Key Laboratory of Quantum State Construction and Manipulation (Ministry of Education), Renmin University of China, Beijing, 100872, China*

³*Theoretical Division and Center for Integrated Nanotechnologies, Los Alamos National Laboratory, Los Alamos, New Mexico 87545, USA*

⁴*Department of Physics & Astronomy, Rice Center for Quantum Materials, Rice University, Houston, Texas 77005, USA*

Strong correlations lead to emergent excitations at low energies. When combined with symmetry constraints, they may produce topological electronic states near the Fermi energy. Within this general framework, here we address the topological features in iron-based superconductors. We examine the effects of orbital-selective correlations on the band inversion in the iron chalcogenide $\text{FeSe}_x\text{Te}_{1-x}$ near its doping of optimal superconductivity, within a multi-orbital model and using a $U(1)$ slave spin theory. The orbital selectivity of the quasiparticle spectral weight, along with its counterpart of the energy level renormalization, leads to a band inversion and Dirac node formation pinned to the immediate vicinity of the Fermi energy. Our work demonstrates both the naturalness and robustness of the topological properties in $\text{FeSe}_x\text{Te}_{1-x}$, and uncovers a new setting in which strong correlations and space-group symmetry cooperate in generating strongly correlated electronic topology.

Introduction. Since its discovery [1], iron-based superconductors (FeSCs) have attracted extensive research interest because of their unconventional high-temperature superconductivity and a rich landscape of electronic orders [2–10]. These properties originate from electron correlations, which can be strongly orbital dependent in many FeSCs [11–25]. The Hund’s rule coupling plays a crucial role in suppressing the interorbital correlations [11, 14] and drives the system towards an orbital-selective Mott phase. Strong orbital selectivity causes a substantial renormalization of the band structure in the normal state, giving rise to a large effective mass enhancement [17, 25, 26] and reconstruction of band structure and Fermi surface [26, 27], and stabilizing orbital-selective pairing states in the superconducting state [28–31]. It has been recognized that strong orbital selectivity is universal in iron chalcogenides [25], and an orbital-selective Mott transition (OSMT) can be approached by successively increasing the Te concentration in $\text{FeSe}_x\text{Te}_{1-x}$ [26]. The orbital selectivity can be quantified by the difference in the enhancement of the effective mass m^* from the band mass m_b . For $\text{FeSe}_x\text{Te}_{1-x}$ near $x = 0.5$, the enhancement factor m^*/m_b is very large for $3d_{xy}$ states (~ 15) and moderate for $3d_{xz/yz}$ states (~ 4), which dominate over the e_g states near the Fermi energy [3, 6, 24–26].

The FeSCs are being pursued as promising materials for topological superconductivity and, thus, a candidate platform for fault-tolerant quantum computation [32, 33]. In the iron chalcogenides $\text{FeSe}_x\text{Te}_{1-x}$ near $x \approx 0.5$, there has been emerging experimental evidence for topological surface states and Majorana zero modes in vortex cores in the superconducting state [34, 35]. Instead of utilizing intrinsic unconventional pairing such as chiral p -wave pairing, as being pursued in correlated materials such as

UTe_2 [36], here one relies on the (in-situ) proximity between superconductivity and band inversion [37]. This mechanism requires that the topological band inversion takes place in the immediate vicinity of the Fermi energy [38]. The experimental evidence is consistent with this requirement, with the surface Dirac states evinced within about 20 meV of the Fermi energy [39–44]. However, most existing theories on the non-trivial band topology [45–50] are anchored by the density functional theory (DFT) calculations, which found band inversion much further away from the Fermi energy, by an order of magnitude [45, 46].

In this Letter, we address the above issue by showing that the orbital-selective Mott correlations produce single-particle states that are pinned very close to E_F and retain band inversion and Dirac nodes along the Γ - Z (k_z) direction. As such, the energies of topological gap and Dirac node locations as measured with respect to the Fermi energy are very small, within about 20 meV, which is consistent both with the experimental observation and with the requirement for surface topological superconductivity. We reach this conclusion by investigating a multi-orbital Hubbard model including both Fe d and Se/Te p orbitals for $\text{FeSe}_x\text{Te}_{1-x}$, using the $U(1)$ slave spin theory [51, 52]. The band inversion takes place between a p_z - d_{xy} hybridized band and a $d_{xz/yz}$ band, leading to a topological insulator-like feature in the presence of the spin-orbit coupling/ While above the gap, a Dirac node emerges which reflects the protection of a C_{4z} rotational symmetry along the high symmetry line Γ - Z . Still, we show that this picture has a degree of robustness, because the orbital selective renormalization involves not only the quasiparticle spectral weight but also the energy levels. The two types of renormalization effects cause opposite shifts of the d_{xy} and $d_{xz/yz}$ bands, and it follows

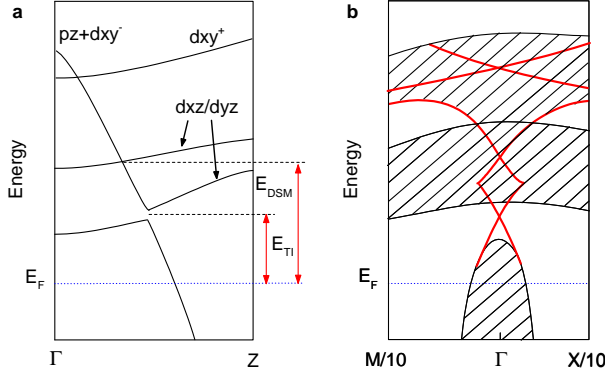


FIG. 1. (Color online) **a**: Sketch of the band inversion that yields a topological-insulator gap and symmetry-protected Dirac crossing along the Γ -Z direction of the BZ in $\text{FeSe}_x\text{Te}_{1-x}$ at $x = 0.5$, defining two energy scales, E_{TI} and E_{DSM} . **b**: Corresponding topological surface states (solid lines) near the Γ point. The bulk bands are represented by the shading.

that the Fermi-energy-pinned band inversion and Dirac node formation occur over a wide interaction parameter range. When the interaction becomes too large and the system approaches an OSMT, we find a topological phase transition to where the renormalized bands can no longer invert. Our results illustrate a general principle, namely (orbital-selective) electron correlations cooperate with space group symmetry to produce correlated topological properties [53].

Qualitative picture. The overall picture is illustrated in Fig. 1a. A topological gap caused by the band inversion is located at E_{TI} away from the Fermi energy (E_F), while a Dirac node protected by the C_{4z} lattice rotational symmetry is at E_{DSM} ; each gives rise to a surface Dirac cone as depicted in Fig. 1b.

From the DFT calculation, the band inversion is between a p_z band and the $d_{xz/yz}$ bands along the Γ -Z (k_z) direction of the Brillouin zone (BZ). At the Γ point the p_z band is located at a higher energy than the $d_{xz/yz}$ bands. This is inverted at the Z point as the p_z band is strongly dispersive along the k_z direction. A finite spin-orbit coupling (SOC) causes a splitting of the doubly degenerate $d_{xz/yz}$ bands, and leads to a bulk gap between the p_z band and one of the $d_{xz/yz}$ bands. The opposite parities of the p_z and $d_{xz/yz}$ bands give rise to topological surface states. A Dirac cone-type surface state appears at the Γ point on the (001) surface. This is similar to the case of a topological insulator (TI) which has a bulk gap and a Dirac cone-type gapless surface state. Above the bulk gap, the p_z band crosses the other $d_{xz/yz}$ band at a higher energy. The level crossing is protected by the C_{4z} rotational symmetry of the lattice, and this leads to another Dirac semi-metal (DSM)-type surface state at a slightly higher energy. In DFT calculations, the energy positions of the bulk gap and the Dirac cones are about 200 meV

higher than the Fermi energy E_F (c.f. Figs. 2a). The role of the electron correlations on the band topological features has been discussed [54], and recent calculations based on DFT in combination with dynamical mean-field theory (DMFT) have suggested that the overall correlation effects may move such features towards the Fermi energy [55].

Model and method. We study a multiorbital Hubbard model for $\text{FeSe}_x\text{Te}_{1-x}$, which includes the five 3d orbitals of Fe and the p_z orbital of Se/Te. The model Hamiltonian reads as

$$H = H_{\text{TB}} + H_{\text{soc}} + H_{\text{int}}. \quad (1)$$

Here, H_{TB} is a tight-binding Hamiltonian with tetragonal lattice symmetry.

$$H_{\text{TB}} = \frac{1}{2} \sum_{ij\alpha\beta\sigma} t_{ij}^{\alpha\beta} d_{i\alpha\sigma}^\dagger d_{j\beta\sigma} + \sum_{i\alpha\sigma} (\epsilon_\alpha - \mu) d_{i\alpha\sigma}^\dagger d_{i\alpha\sigma} + \sum_{il\alpha\sigma} t_{li}^{p\alpha} (p_{l\sigma}^\dagger d_{i\alpha\sigma} + d_{i\alpha\sigma}^\dagger p_{l\sigma}) + \sum_{l\sigma} (\epsilon_p - \mu) p_{l\sigma}^\dagger p_{l\sigma}, \quad (2)$$

where $d_{i\alpha\sigma}^\dagger$ creates an electron in orbital α ($\alpha = 1, \dots, 5$ denoting xz , yz , $x^2 - y^2$, xy , and $3z^2 - r^2$ orbitals, respectively) with spin σ at site i , ϵ_α refers to the d -orbital energy level associated with the crystal field splittings, $p_{l\sigma}^\dagger$ creates an electron in the p_z orbital of Se/Te, ϵ_p denotes the p_z -orbital onsite energy, and μ is the chemical potential. The tight-binding parameters $t_{ij}^{\alpha\beta}$, $t_{li}^{p\alpha}$, ϵ_α , and ϵ_p can be obtained by fitting the calculated DFT band structure and projecting to a 12-orbital basis including the Fe 3d orbitals and the p_z orbital of Se/Te as described in Supplemental Material (SM) [56]. In addition, the atomic SOC term in the d -orbital sector is $H_{\text{soc}} = \frac{1}{2} \lambda_{\text{soc}}^0 \sum_{i\alpha\beta\sigma\sigma'} (\mathbf{L} \cdot \boldsymbol{\tau})_{\alpha\sigma, \beta\sigma'} d_{i\alpha\sigma}^\dagger d_{i\beta\sigma'}$, where \mathbf{L} denotes the orbital angular momentum operator and $\boldsymbol{\tau}$ refers to the Pauli matrices. A bare value of the SOC $\lambda_{\text{soc}}^0 = 60$ meV is taken, which will be renormalized by interactions. We adjust the chemical potential so that the total electron density is 16 per unit cell, which includes 12 electrons on Fe sites and 4 electrons on Se/Te sites in a unit cell containing two Fe and two Se/Te ions. The on-site interaction H_{int} reads

$$H_{\text{int}} = \frac{U}{2} \sum_{i,\alpha,\sigma} n_{i\alpha\sigma} n_{i\alpha\bar{\sigma}} + \sum_{i,\alpha<\beta,\sigma} \{ U' n_{i\alpha\sigma} n_{i\beta\bar{\sigma}} + (U' - J_H) n_{i\alpha\sigma} n_{i\beta\sigma} - J_H (d_{i\alpha\sigma}^\dagger d_{i\alpha\bar{\sigma}} d_{i\beta\bar{\sigma}}^\dagger d_{i\beta\sigma} + d_{i\alpha\sigma}^\dagger d_{i\alpha\bar{\sigma}}^\dagger d_{i\beta\sigma} d_{i\beta\bar{\sigma}}) \} \quad (3)$$

where $n_{i\alpha\sigma} = d_{i\alpha\sigma}^\dagger d_{i\alpha\sigma}$. Here, U , U' , and J_H , respectively denote the intra- and inter-orbital repulsion and the Hund's rule coupling, and $U' = U - 2J_H$ is taken [57]. In the calculation, we fix $J_H/U = 0.25$ and neglect interactions in the p orbitals.

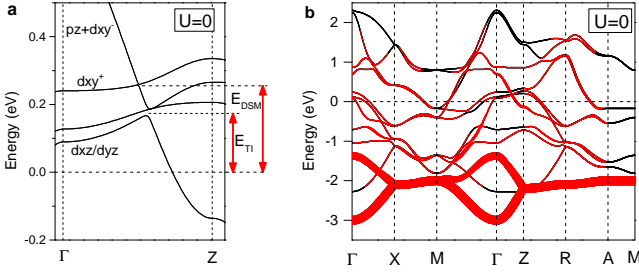


FIG. 2. (Color online) Band structure of the 12-orbital Hubbard model in the non-interacting limit with $\lambda_{\text{SOC}}^0 = 60$ meV. **a:** The band structure near the Fermi energy E_F (which is set to be zero) along the Γ -Z direction of the BZ showing the band inversion, which causes a bulk gap at energy position $E_{\text{TI}} \approx 170$ meV and a Dirac level crossing at $E_{\text{DSM}} \approx 260$ meV. **b:** Full band structure of the 12-orbital model along high symmetric directions of the BZ. The thickness of the red line is proportional to the p_z orbital weight of the bands.

The correlation effects of the above model are investigated by using a $U(1)$ slave-spin theory [51, 52]. In the $U(1)$ slave-spin theory, the d -electron operator is rewritten as $d_{i\alpha\sigma}^\dagger = S_{i\alpha\sigma}^+ f_{i\alpha\sigma}^\dagger$, where $S_{i\alpha\sigma}^+$ ($f_{i\alpha\sigma}^\dagger$) is a quantum $S = 1/2$ spin (fermionic spinon) operator introduced to carry the electron's charge (spin) degree of freedom, and $S_{i\alpha\sigma}^z = f_{i\alpha\sigma}^\dagger f_{i\alpha\sigma} - \frac{1}{2}$ is a local constraint. At the saddle-point level, we employ a Lagrange multiplier λ_α to handle the constraint, and decompose the slave-spin and spinon operators. In this way, the Hamiltonian in Eqn. (1) is solved by determining λ_α and the quasiparticle spectral weight $Z_\alpha \propto |\langle S_\alpha^+ \rangle|^2$ self-consistently [51, 52].

Band topology under orbital-selective correlations. We focus on studying the band structure of the above model for $\text{FeSe}_x\text{Te}_{1-x}$ at $x = 0.5$, where the non-trivial band topology is observed in experiments. Fig. 2b shows the band structure of the 12-orbital model with a finite SOC in the non-interacting limit $U = J_H = 0$. Bands across the Fermi energy have mainly the d -orbital character except one band along the Γ -Z direction (shown in red), in which the dominant orbital character is p_z . This band involves the p_z orbital hybridizing with the d_{xy} orbital and has an odd parity. As shown in Fig. 2a, this band crosses another d_{xy} band with even parity (d_{xy}^+) and two $d_{xz/yz}$ hybridized bands in turn. In particular, the crossing between the odd-parity $p_z + d_{xy}^-$ band and one even-parity $d_{xz/yz}$ band identifies a band inversion. The latter gives rise to Z_2 band topology as in a topological insulator (TI): In the presence of the SOC, a bulk gap develops whereas the surface mode keeps as a gapless Dirac cone (see below). In the calculation, the other $d_{xz/yz}$ band split by the SOC lies in the bulk gap. Slightly above the bulk gap, the $p_z + d_{xy}^-$ band crosses the d_{xy}^+ band, leading to a Dirac semi-metal (DSM) feature. We can define two characteristic energies of the band topology: The energy position (to E_F) of the bulk gap $E_{\text{TI}} \approx 170$ meV,

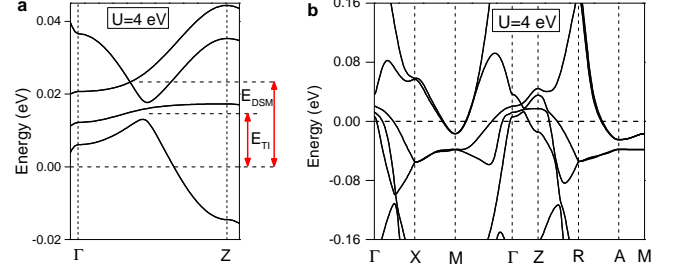


FIG. 3. (Color online) **a:** Renormalized band structure near the Fermi energy E_F for $U = 4$ eV, along Γ -Z showing the band inversion, with $E_{\text{TI}} \approx 14$ meV and a Dirac level crossing at $E_{\text{DSM}} \approx 22$ meV. **b:** The corresponding band structure along high symmetric directions of the BZ.

and the energy of the DSM-like crossing is $E_{\text{DSM}} \approx 260$ meV. Although the band topology is present in the non-interacting limit, the characteristic energies are too large compared to those found in experiments.

We now consider the effects of electron correlations. The evolution of the orbital resolved quasiparticle spectral weight Z_α with U , for a typical ratio of $J_H/U = 0.25$, is shown in Fig. S2. At $U \sim 2 - 3$ eV, the system crosses over to a strongly correlated metal, where Z_α in all orbitals drop rapidly and become strongly orbital selective. This feature is universal for FeSCs. In the strongly correlated metal phase, the d_{xy} orbital is the most strongly correlated, with $Z \lesssim 0.1$ for $U \gtrsim 4$ eV. As expected (see Fig. 3b), the bands are highly renormalized. We find the band inversion persists under such a strong orbital-selective correlation up to $U \approx 10$ eV. Comparing the band structure at $U = 4$ eV in Fig. 3a to that at $U = 0$ in Fig. 2, the characteristic energies are very close to the the Fermi energy: $E_{\text{TI}} \approx 14$ meV and $E_{\text{DSM}} \approx 22$ meV at $U = 4$ eV.

To demonstrate the band topology, we calculate the surface state spectrum by taking a slab-like lattice geometry. As shown in Fig. 4, for both $U = 0$ and $U = 4$ eV, a clear Dirac cone shows up in the bulk gap at the Γ point. Slightly above in energy, there is another Dirac cone that is associated with the DSM feature of the bulk spectrum. The correlation effects reduce the energy positions of the Dirac cones by about one order of magnitude. For $U = 4$ eV, the calculated Dirac surface state is only about 15 meV above the Fermi level. A slight electron doping in the system may further push this energy to be below E_F .

Band shifts caused by orbital-selective correlation and the robustness of band inversion. The orbital-selective correlations push the $p_z + d_{xy}^-$ band towards E_F . This would make the energy position of this band lower than those of the $d_{xz/yz}$ bands at the Γ point, and hence remove the band inversion. Nonetheless, our calculation shows that the band inversion persists over a wide range of interaction up to about $U = 10$ eV. To understand

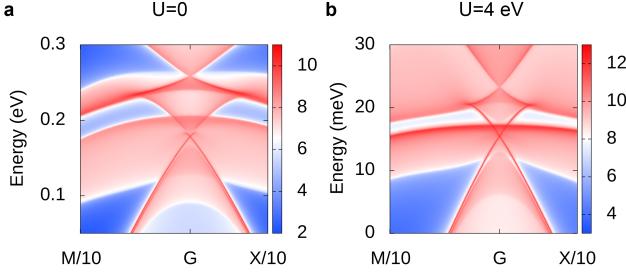


FIG. 4. (Color online) Topological surface states showing the Dirac cone features of the model on the (001) surface, at $U = 0$ (in **a**) and $U = 4$ eV (in **b**).

the robustness of the band inversion in the model, we examine the energy positions of the $p_z + d_{xy}^-$ and $d_{xz/yz}$ bands at Γ point for $U = 0$ and $U = 4$ eV, respectively. The energy of the $p_z + d_{xy}^-$ band is renormalized from $E \approx 0.8$ eV to $E \approx 0.04$ eV at $U = 4$ eV. The renormalization factor is about 20, which is close to the value of $1/Z_{xy} \approx 18$ at $U = 4$ eV. On the other hand, the energy of the $d_{xz/yz}$ bands (when neglecting the splitting by spin-orbit coupling) is renormalized from $E \approx 0.1$ eV to $E \approx 0.01$ eV, *eg.*, by a factor of 10. This factor is almost twice as large as $1/Z_{xz/yz} \approx 6$ at $U = 4$ eV. This unusually strong renormalization of the $d_{xz/yz}$ band energy helps keep the $d_{xz/yz}$ band lower than the $p_z + d_{xy}^-$ band at Γ point, and hence maintain the band inversion.

Near the Γ point, the hybridization between the d_{xy} and $d_{xz/yz}$ orbitals is weak. The energy of a band with a dominant α orbital at a wave vector k is then written as $E_{\alpha k} = \epsilon_{\alpha} + \xi_{\alpha}(k)$, where ϵ_{α} is the onsite energy associated with the crystal field splittings, and $\xi_{\alpha}(k)$ is the dispersive part of the band which is obtained from Fourier transformation of hopping parameters. Under electron correlation the energy is renormalized to $\tilde{E}_{\alpha k} = Z'_{\alpha}\epsilon_{\alpha} + Z_{\alpha}\xi_{\alpha}(k)$, where Z_{α} is the quasiparticle spectral weight and Z'_{α} is a renormalization factor for the onsite energy ϵ_{α} [27]. In a system with strong orbital selectivity, Z' and Z may differ sizeably, given that Z' reflects the redistribution of electron among different orbitals [27] (see Fig. S3 of SM [56]). Rewriting $\tilde{E}_{\alpha k} = Z_{\alpha}E_{\alpha k} + (Z'_{\alpha} - Z_{\alpha})\epsilon_{\alpha}$, it can be seen that the difference between Z and Z' generates an additional energy shift of a band. It has been shown that this leads to a reconstruction of the bandstructure and Fermi surface in LiFeAs [27]. In the case of $\text{FeSe}_x\text{Te}_{1-x}$, we show that this effect helps stabilize the band inversion under strong orbital selective correlation. By comparison, we find $Z_{xy} \approx 0.056$ and $Z'_{xy} \approx 0.017$. Together with $\epsilon_{xy} \approx -0.137$ eV, this yields a small *positive* shift of about 0.005 eV. For the $d_{xz/yz}$ bands, $Z_{xz/yz} \approx 0.164$, $Z'_{xz/yz} \approx -0.008$, and $\epsilon_{xz/yz} \approx 0.051$ eV, which lead to a *negative* shift of about 0.009 eV. This significant energy downshift accounts for the unusually strong renormaliza-

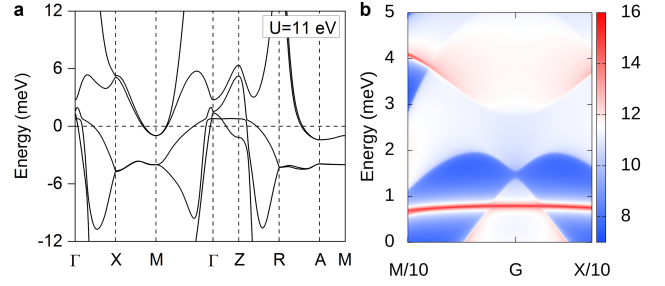


FIG. 5. (Color online) **a**: Band structure along high symmetric directions of the BZ at $U = 11$ eV, where the bands no longer invert. **b**: The corresponding surface state calculation at $U = 11$ eV, showing that the topological surface states disappear under extreme orbital selectivity.

tion of the $d_{xz/yz}$ band energy. More importantly, the energy shifts in the d_{xy} and $d_{xz/yz}$ bands are in *opposite* directions. This partially cancels the effect of strong bandwidth renormalization in the d_{xy} band, making the energy of the d_{xy} band at Γ point higher than that of the $d_{xz/yz}$ bands. As such, the band inversion is stabilized over a wide range of interactions, up to about $U \approx 10$ eV.

Topological phase transition under strong orbital selectivity. Further increasing electron correlations to $U > 10$ eV, the difference between Z and Z' becomes vanishing. In this strong orbital-selective limit, we expect the $p_z + d_{xy}^-$ band is further renormalized toward E_F . Without the additional energy shifts caused by Z' , its band energy at Γ point should eventually be pushed to lower than that of the $d_{xz/yz}$ bands, and the band inversion should be removed. We test this idea by taking $U = 11$ eV, where $Z_{xy} \approx 0.002$, which is very close to an OSMT. As shown in Fig. 5a, the $p_z + d_{xy}^-$ band is indeed lower in energy than the $d_{xz/yz}$ bands at both Γ and Z points. As a result, the band inversion is removed and the band topology then becomes trivial. The Dirac cone features disappear in the surface spectrum and full gaps open at the Γ point, as seen in Fig. 5b. Such a drastic change of the band topology indicates that there is a topological phase transition under strong orbital selectivity at $U \approx 11$ eV.

Discussion and conclusions. We have shown how orbital-selective correlations lead to a topological band inversion and Dirac node that are pinned to the immediate vicinity of the Fermi energy. The strong correlations of both the d_{xy} and $d_{xz/yz}$ orbitals make the band topological features robust over a wide range of interactions. Our results provide a natural explanation to the observed topological surface states in $\text{FeSe}_x\text{Te}_{1-x}$ and other FeSCs [40, 41]. More generally, the cooperation of strong correlations and space-group symmetry has been advanced as a design rule for strongly correlated electronic topology [53], and our work showcases the iron

chalcogenide superconductors as a new platform for applying this principle.

We thank Lei Chen, Chandan Setty, Shouvik Sur, and Ming Yi for useful discussions. This work has in part been supported by the National Science Foundation of China Grant No. 12174441. Work at Rice was primarily supported by the U.S. Department of Energy, Office of Science, Basic Energy Sciences, under Award No. DE-SC0018197, and by the Robert A. Welch Foundation Grant No. C-1411. Work at Los Alamos was carried out under the auspices of the U.S. DOE NNSA under Contract No. 89233218CNA000001. It was supported by LANL LDRD Program and in part by the Center for Integrated Nanotechnologies, a U.S. DOE BES user facility. Q.S. acknowledges the hospitality of the Kavli Institute for Theoretical Physics, supported in part by the National Science Foundation under Grant No. NSF PHY-1748958, during the program “A Quantum Universe in a Crystal: Symmetry and Topology across the Correlation Spectrum”, as well as the hospitality of the Aspen Center for Physics, which is supported by NSF grant No. PHY-1607611.

Note added: After completing this work, we learnt of another work [62], in which the effect of the orbital-selective Mott correlations on the band topology of $\text{FeSe}_{0.5}\text{Te}_{0.5}$ is studied using the DMFT method.

* rong.yu@ruc.edu.cn

† jxzhu@lanl.gov

‡ qmsi@rice.edu

- [1] Y. Kamihara, T. Watanabe, M. Hirano, and H. Hosono, “Iron-Based Layered Superconductor $\text{La}[\text{O}_{1-x}\text{F}_x]\text{FeAs}$ ($x = 0.05\text{--}0.12$) with $T_c = 26$ K”, *J. Am. Chem. Soc.* **130**, 3296 (2008).
- [2] Q. Si and N. E. Hussey, “Iron-based superconductors: Teenage, complex, challenging”, *Phys. Today* **76** (5), 34 (2023).
- [3] M. Yi, Y. Zhang, Z.-X. Shen, and D.-H. Lu, “Role of the orbital degree of freedom in iron-based superconductors”, *npj Quant. Mater.* **2**, 57 (2017).
- [4] E. Bascones, B. Valenzuela, and M. J. Calderón, “Magnetic interactions in iron superconductors: A review”, *Comptes Rendus Physique* **17**, 36 (2016).
- [5] P. J. Hirschfeld, “Gap Symmetry and Structure to Reveal the Pairing Mechanism in Fe-based Superconductors”, *Comptes Rendus Physique* **17**, 197 (2016).
- [6] Q. Si, R. Yu and E. Abrahams, “High Temperature Superconductivity in Iron Pnictides and Chalcogenides”, *Nat. Rev. Mater.* **1**, 16017 (2016).
- [7] P. Dai, “Antiferromagnetic order and spin dynamics in iron-based Superconductors”, *Rev. Mod. Phys.* **87**, 855–896 (2015).
- [8] E. Dagotto, “The Unexpected Properties of Alkali Metal Iron Selenide Superconductors”, *Rev. Mod. Phys.* **85**, 849 (2013).
- [9] F. Wang and D.-H. Lee, “The Electron-Pairing Mechanism of Iron-Based Superconductors”, *Science* **332**, 200–204 (2011).
- [10] D. C. Johnston, “The puzzle of high temperature superconductivity in layered iron pnictides and chalcogenides”, *Adv. Phys.* **59**, 803–1061 (2010).
- [11] R. Yu and Q. Si, “Mott Transition in MultiOrbital Models for Iron Pnictides”, *Phys. Rev. B* **84**, 235115 (2011).
- [12] Z. P. Yin, K. Haule, and G. Kotliar, “Magnetism and charge dynamics in iron pnictides”, *Nat. Phys.* **7**, 294(2011).
- [13] R. Yu and Q. Si, “Orbital-Selective Mott Phase in Multiorbital Models for Alkaline Iron Selenides $\text{K}_{1-x}\text{Fe}_{2-y}\text{Se}_2$ ”, *Phys. Rev. Lett.* **110**, 146402 (2013).
- [14] L. de’ Medici, G. Giovannetti, and M. Capone, “Selective Mott Physics as a Key to Iron Superconductors”, *Phys. Rev. Lett.* **112**, 177001 (2014).
- [15] S. Backes, H. O. Jeschke, and R. Valenti, “Microscopic nature of correlations in multiorbital AFe_2As_2 ($A = \text{K}, \text{Rb}, \text{Cs}$): Hund’s coupling versus Coulomb repulsion”, *Phys. Rev. B* **92**, 195128 (2015).
- [16] N. Patel, A. Nocera, G. Alvarez, A. Moreo, S. Johnston, and E. Dagotto, “Fingerprints of an orbital-selective Mott phase in the block magnetic state of BaFe_2Se_3 ladders”, *Commun. Phys.* **2**, 1 (2019).
- [17] M. Yi, D. H. Lu, R. Yu, S. C. Riggs, J.-H. Chu, B. Lv, Z. K. Liu, M. Lu, Y. T. Cui, M. Hashimoto, S.-K. Mo, Z. Hussain, C. W. Chu, I. R. Fisher, Q. Si, and Z.-X. Shen, “Observation of Temperature-Induced Crossover to an Orbital-Selective Mott Phase in $\text{A}_x\text{Fe}_{2-y}\text{Se}_2$ ($A=\text{K}, \text{Rb}$) Superconductors”, *Phys. Rev. Lett.* **110**, 067003 (2013).
- [18] Z. Wang, M. Schmidt, J. Fischer, V. Tsurkan, M. Greger, D. Vollhardt, A. Loidl, and J. Deisenhofer, “Orbital-selective metal-insulator transition and gap formation above T_c in superconducting $\text{Rb}_{1-x}\text{Fe}_{2-y}\text{Se}_2$ ”, *Nat. Commun.* **5**, 3202 (2014).
- [19] X. Ding, Y. Pan, H. Yang, and H.-H. Wen, “Strong and nonmonotonic temperature dependence of Hall coefficient in superconducting $\text{K}_x\text{Fe}_{2-y}\text{Se}_2$ single crystals”, *Phys. Rev. B* **89**, 224515(2014).
- [20] M. Wang, M. Yi, H. Cao, C. de la Cruz, S. K. Mo, Q. Z. Huang, E. B.-Courchesne, P. Dai, D. H. Lee, Z. X. Shen, and R. J. Birgeneau, “Mott localization in a pure stripe antiferromagnet $\text{Rb}_{1-\delta}\text{Fe}_{1.5-\sigma}\text{S}_2$ ”, *Phys. Rev. B* **92**, 121101(R) (2015).
- [21] X. H. Niu, S. D. Chen, J. Jiang, Z. R. Ye, T. L. Yu, D. F. Xu, M. Xu, Y. Feng, Y. J. Yan, B. P. Xie, J. Zhao, D. C. Gu, L. L. Sun, Q. Mao, H. Wang, M. Fang, C. J. Zhang, J. P. Hu, Z. Sun, and D. L. Feng “A unifying phase diagram with correlation-driven superconductor-to-insulator transition for the 122” series of iron chalcogenides”, *Phys. Rev. B* **93**, 054516 (2016).
- [22] M. Hiraishi, K. M. Kojima, H. Okabe, S. Takeshita, A. Koda, R. Kadono, R. Khasanov, S. Iimura, S. Matsui, H. Hosono, “Magnetism driven by strong electronic correlation in the heavily carrier-doped iron oxypnictide $\text{LaFeAsO}_{0.49}\text{H}_{0.51}$ ”, *Phys. Rev. B* **101**, 174414 (2020).
- [23] J. Si, G.-Y. Chen, Q. Li, X. Zhu, H. Yang, and H.-H. Wen, “Unconventional Superconductivity Induced by Suppressing an Iron-Selenium-Based Mott Insulator $\text{CsFe}_{4-x}\text{Se}_4$ ”, *Phys. Rev. X* **10**, 041008 (2020).
- [24] Z.-K. Liu, M. Yi, Y. Zhang, J. Hu, R. Yu, J.-X. Zhu, R.-H. He, Y. L. Chen, M. Hashimoto, R. G. Moore, S.-K. Mo, Z. Hussain, Q. Si, Z. Q. Mao, D. H. Lu, and Z.-X. Shen, “Experimental observation of incoherent-coherent crossover and orbital-dependent band renormalization in

- iron chalcogenide superconductors”, *Phys. Rev. B* **92**, 235138 (2015).
- [25] M. Yi, Z.-K. Liu, Y. Zhang, R. Yu, J.-X. Zhu, J. J. Lee, R. G. Moore, F. T. Schmitt, W. Li, S. C. Riggs, J.-H. Chu, B. Lv, J. Hu, T. J. Liu, M. Hashimoto, S.-K. Mo, Z. Hussain, Z. Q. Mao, C. W. Chu, I. R. Fisher, Q. Si, Z.-X. Shen, and D. H. Lu, “Observation of universal strong orbital-dependent correlation effects in iron chalcogenides”, *Nat. Commun.* **6**, 7777 (2015).
- [26] J. Huang *et al.*, “Correlation-Driven Electronic Reconstruction in $\text{FeTe}_{1-x}\text{Se}_x$ ”, *Commun. Phys.* **5**, 29 (2022).
- [27] H. Lin, R. Yu, J.-X. Zhu, and Q. Si, arXiv:2101.05598.
- [28] R. Yu, J.-X. Zhu, and Q. Si, “Orbital-selective superconductivity, gap anisotropy, and spin resonance excitations in a multiorbital t - J_1 - J_2 model for iron pnictides”, *Phys. Rev. B* **89**, 024509 (2014).
- [29] Z. P. Yin, K. Haule, and G. Kotliar, “Spin dynamics and orbital-antiphase pairing symmetry in iron-based superconductors”, *Nat. Phys.* **10**, 845 (2014).
- [30] T. Ong, P. Coleman, J. Schmalian, “Concealed d-wave pairs in the s condensate of iron-based superconductors”, *Proc. Nat. Acad. Sci. (USA)* **113**, 5486 (2016).
- [31] E. M. Nica, R. Yu, and Q. Si, “Orbital selective pairing and superconductivity in iron selenides”, *npj Quant. Mater.* **2**, 24 (2017).
- [32] A. Y. Kitaev, “Fault-tolerant quantum computation by anyons”, *Ann. Phys. (Amsterdam)* **303**, 2 (2003).
- [33] C. Nayak, S. H. Simon, A. Stern, M. Freedman, S. Das Sarma, “Non-Abelian anyons and topological quantum computation”, *Rev. Mod. Phys.* **80**, 1083-1159 (2008).
- [34] D. Wang, L. Kong, P. Fan, H. Chen, S. Zhu, W. Liu, L. Cao, Y. Sun, S. Du, J. Schneeloch, R. Zhong, G. Gu, L. Fu, H. Ding, and H.-J. Gao, “Evidence for Majorana bound states in an iron-based superconductor”, *Science* **362**, 333-335 (2018).
- [35] S. Zhu, L. Kong, L. Cao, H. Chen, M. Papaj, S. Du, Y. Xing, W. Liu, D. Wang, C. Shen, F. Yang, J. Schneeloch, R. Zhong, G. Gu, L. Fu, Y.-Y. Zhang, H. Ding, and H.-J. Gao, “Nearly quantized conductance plateau of vortex zero mode in an iron-based superconductor”, *Science* **367**, 189-192 (2020).
- [36] L. Jiao, S. Howard, S. Ran, Z. Wang, J. O. Rodriguez, M. Sigrist, Z. Wang, N. P. Butch, and V. Madhavan, “Chiral superconductivity in heavy-fermion metal UTe_2 ”, *Nature* **579**, 523 (2020).
- [37] L. Fu and C. L. Kane, “Superconducting Proximity Effect and Majorana Fermions at the Surface of a Topological Insulator”, *Phys. Rev. Lett.* **100**, 096407 (2008).
- [38] L.-H. Hu, X. Wu, C.-X. Liu, and R.-X. Zhang, “Competing Vortex Topologies in Iron-Based Superconductors”, *Phys. Rev. Lett.* **129**, 277001 (2022).
- [39] P. Zhang, K. Yaji, T. Hashimoto, Y. Ota, T. Kondo, K. Okazaki, Z. Wang, J. Wen, G. D. Gu, H. Ding, and S. Shin, “Observation of topological superconductivity on the surface of an iron-based superconductor”, *Science* **360**, 182-186 (2018).
- [40] P. Zhang, Z. Wang, X. Wu, K. Yaji, Y. Ishida, Y. Kohama, G. Dai, Y. Sun, C. Bareille, K. Kuroda, T. Kondo, K. Okazaki, K. Kindo, X. Wang, C. Jin, J. Hu, R. Thomale, K. Sumida, S. Wu, K. Miyamoto, T. Okuda, H. Ding, G. D. Gu, T. Tamegai, T. Kawakami, M. Sato, and S. Shin, “Multiple topological states in iron-based superconductors”, *Nat. Phys.* **15**, 41 (2019).
- [41] C. Chen, Q. Liu, T. Z. Zhang, D. Li, P. P. Shen, X. L. Dong, Z.-X. Zhao, T. Zhang, and D. L. Feng, “Quantized Conductance of Majorana Zero Mode in the Vortex of the Topological Superconductor $(\text{Li}_{0.84}\text{Fe}_{0.16})\text{OHFeSe}$ ”, *Chin. Phys. Lett.* **36**, 057403 (2019).
- [42] H. Lohani, T. Hazra, A. Ribak, Y. Nitzav, H. Fu, B. Yan, M. Randeria, and A. Kanigel, “Band inversion and topology of the bulk electronic structure in $\text{FeSe}_{0.45}\text{Te}_{0.55}$ ”, *Phys. Rev. B* **101**, 245146 (2020).
- [43] R. P. Day *et al.*, “Three-dimensional electronic structure of LiFeAs ”, *Phys. Rev. B* **105**, 155142 (2022).
- [44] M. Li, G. Li, L. Cao, X. Zhou, X. Wang, C. Jin, C.-K. Chiu, S. J. Pennycook, Z. Wang, and H.-J. Gao, “Ordered and tunable Majorana-zero-mode lattice in naturally strained LiFeAs ”, *Nature* **606**, 890 (2022).
- [45] Z. Wang, P. Zhang, G. Xu, L. K. Zeng, H. Miao, X. Xu, T. Qian, H. Weng, P. Richard, A. V. Fedorov, H. Ding, X. Dai, and Z. Fang, “Topological nature of the $\text{FeSe}_{0.5}\text{Te}_{0.5}$ superconductor”, *Phys. Rev. B* **92**, 115119 (2015).
- [46] Gang Xu, Biao Lian, Peizhe Tang, Xiao-Liang Qi, and Shou-Cheng Zhang, “Topological Superconductivity on the Surface of Fe-Based Superconductors”, *Phys. Rev. Lett.* **117**, 047001 (2016).
- [47] Ning Hao and Jiangping Hu, “Topological quantum states of matter in iron-based superconductors: from concept to material realization”, *Nat. Sci. Rev.* **6**, 213-226 (2019).
- [48] K. Jiang, X. Dai, and Z. Wang, “Quantum Anomalous Vortex and Majorana Zero Mode in Iron-Based Superconductor $\text{Fe}(\text{Te},\text{Se})$ ”, *PHYSICAL REVIEW X* **9**, 011033 (2019).
- [49] R.-X. Zhang, W. S. Cole, and S. Das Sarma, “Helical Hinge Majorana Modes in Iron-Based Superconductors”, *Phys. Rev. Lett.* **122**, 187001 (2019).
- [50] E. J. König and P. Coleman, “Crystalline-Symmetry-Protected Helical Majorana Modes in the Iron Pnictides”, *Phys. Rev. Lett.* **122**, 207001 (2019).
- [51] R. Yu and Q. Si, “ $U(1)$ slave-spin theory and its application to Mott transition in a multiorbital model for iron pnictides”, *Phys. Rev. B* **86**, 085104 (2012).
- [52] R. Yu and Q. Si, “Orbital-selective Mott phase in multiorbital models for iron pnictides and chalcogenides”, *Phys. Rev. B* **96**, 125110 (2017).
- [53] L. Chen, C. Setty, H. Hu, M. G. Vergniory, S. E. Grefe, L. Fischer, X. L. Yan, G. Eguchi, A. Prokofiev, S. Paschen, J. Cano and Q. Si, “Topological semimetal driven by strong correlations and crystalline symmetry”, *Nat. Phys.* **18**, 1341 (2022).
- [54] R. Yu, H. Hu, E. M. Nica, J.-X. Zhu, and Q. Si, “Orbital selectivity in electron correlations and superconducting pairing of iron-based superconductors”, *Front. Phys.* **9**, 978347 (2021).
- [55] X. Ma, G. Wang, R. Liu, T. Yu, Y. Peng, P. Zheng, and Z. P. Yin, “Correlation-corrected band topology and topological surface states in iron-based superconductors”, *Phys. Rev. B* **106**, 115114 (2022).
- [56] See Supplemental Material [<http://link...>] for details about the tight-binding model, which include Refs. [58–61].
- [57] C. Castellani, C. R. Natoli, and J. Ranninger, “Magnetic structure of V_2O_3 in the insulating phase”, *Phys. Rev. B* **18**, 4945 (1978).
- [58] See Quantum ESPRESSO website [<https://www.quantum-espresso.org/>].
- [59] D. R. Hamann, “Optimized norm-conserving Vanderbilt

- pseudopotentials”, Phys. Rev. B **88**, 085117 (2013).
- [60] S. Li and C. D. L. Cruz and Q. Huang and Y. Chen and J. W. Lynn and J. P. Hu and Y. L. Huang and F. C. Hsu and K. W. Yeh and M. K. Wu and P. C. Dai, “First-order magnetic and structural phase transitions in $\text{Fe}_{1+y}\text{Se}_x\text{Te}_{1-x}$ ”, Phys. Rev. B **79**, 054503 (2009).
- [61] G. Pizzi *et al.*, “Wannier90 as a community code: new features and applications”, J. Phys. Cond. Matt. **32**, 165902 (2020).
- [62] M. Kim, S. Choi, W. H. Brito, and G. Kotliar, arXiv:2304.05002.

SUPPLEMENTAL MATERIAL – ORBITAL-SELECTIVE CORRELATIONS FOR TOPOLOGY IN $\text{FeSe}_x\text{Te}_{1-x}$

Details on the tight-binding model

To include the realistic band structure at low energies into our tight-binding modeling, we have first carried out band structure calculations for $\text{FeSe}_x\text{Te}_{1-x}$ (space group: $P4/nmm$) at $x = 0.5$ within the framework of density functional theory (DFT).

We have used the plane wave basis set as implemented in Quantum ESPRESSO code [58]. Norm-conserving pseudopotentials [59] (PPs) and Perdew-Burke-Ernzerhof exchange-correlation functional were used in the calculations. The disorder in $\text{FeSe}_{0.5}\text{Te}_{0.5}$ was described with virtual crystal approximation by mixing the PPs of Se and Te. Experimental lattice parameters ($a = b = 3.79327 \text{ \AA}$, $c = 5.95519 \text{ \AA}$) [60] were used in the simulations. Given that both the Fe t_{2g} and Se/Te p_z orbitals are relevant to the non-trivial band topology, we fit the Wannierized bands with a 12-orbital tight-binding Hamiltonian including the 10 Fe d orbitals and the 2 Se/Te p_z orbitals in the Brillouin zone (BZ) corresponding to the two Fe and two Se/Te unit cell. At this step we have used projected Wannier functions; the procedure of disentanglement was performed with the maximally-localized Wannier functions scheme as implemented in Wannier90 code [61].

The band structure of the 12-orbital tight-binding model compared to the DFT results is shown in Fig. S1. The tight-binding model reproduces a similar band structure of DFT in the energy window of interest, from -3 eV to 2 eV

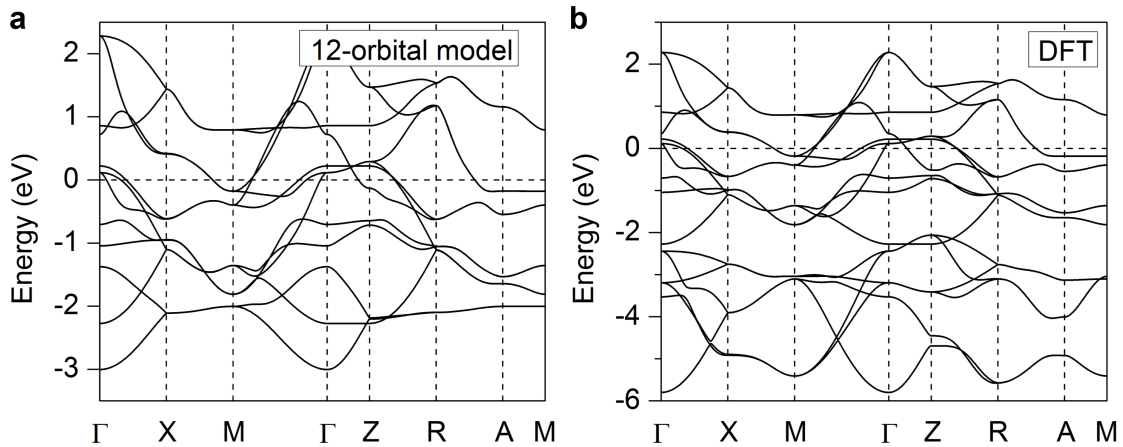


FIG. S1. (Color online) Band structure of $\text{FeSe}_x\text{Te}_{1-x}$ at $x = 0.5$ along high-symmetry directions of the BZ calculated from the 12-orbital tight-binding model (in **a**) and DFT (in **b**).

Details of the orbital-selective correlations and the effects on the band structure

We study the electron correlation effects of the 12-orbital Hubbard model by using the $U(1)$ slave spin theory as described in the main text. Fig. S2 shows the evolution of the quasiparticle spectral weight Z of the Fe $3d$ orbitals with interaction U at $J_H/U = 0.25$. At $U \sim 2-3 \text{ eV}$, the system undergoes a crossover from a weakly correlated metal to a strongly correlated one identified by a rapid drop of Z in all orbitals. In the strongly correlated metallic regime, the system exhibits strong orbital selectivity, with Z values in d_{xy} and $d_{xz/yz}$ orbitals much smaller than those of the e_g orbitals. The crossover and strong orbital selectivity is a well known universal feature of the multiorbital model for the iron chalcogenides, and is driven by a non-trivial interplay of the Hund's coupling and crystal field splitting. Compared to the two e_g orbitals, the three t_{2g} orbitals are located at higher energies, and their occupation numbers are closer to half-filling, as shown in Fig. S3b. As a result, they are closer to a Mott localized state, namely, with smaller quasiparticle spectral weights. This causes strong renormalization of both the d_{xy} and $d_{xz/yz}$ bands, which is important for stabilizing the band inversion while pinning the topological feature close to the Fermi energy. The

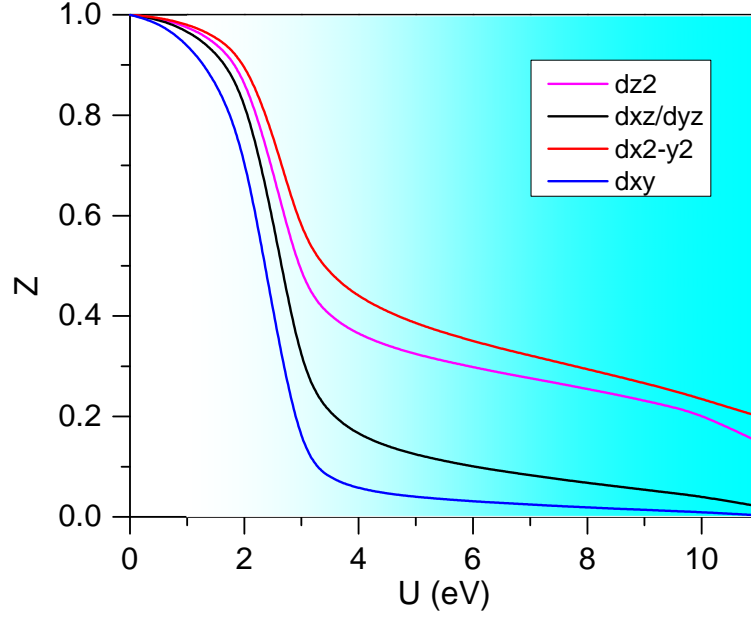


FIG. S2. (Color online) The orbital resolved quasiparticle spectral weight Z as a function of the interaction parameter U of the 12-orbital model. Shading shows the regime where the band inversion and Dirac nodes are pinned close to the Fermi energy.

shading in Fig. S2 shows the range of U where the topological surface states are no more than 30 meV away from the Fermi energy. It spans a wide range from $U \sim 3$ eV to $U \approx 11$ eV in the strongly correlated metal regime.

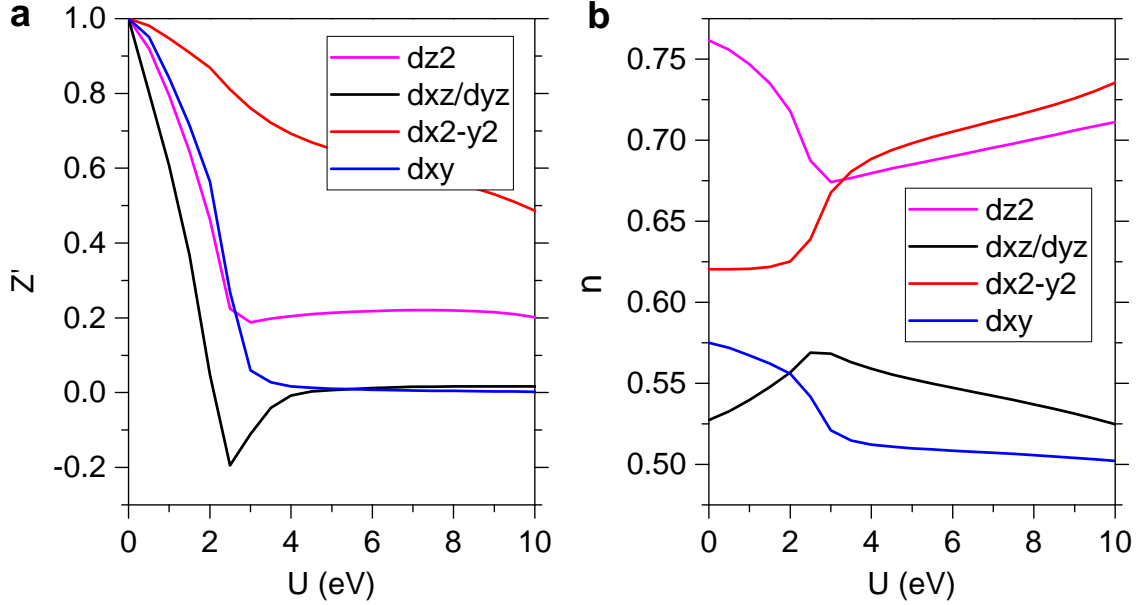


FIG. S3. (Color online) **a**: The renormalization factor Z' of the onsite energy ϵ as a function of U in the 12-orbital model. The renormalization is toward E_F , which is set to 0. Accordingly, Z' can be negative, which corresponds to a renormalized onsite energy below E_F . **b**: Electron occupation number n in each orbital (per spin flavor) vs U in the same model.

As explained in the main text, the d -orbital-based bands have their widths renormalized by the quasiparticle spectral weight Z , whereas the onsite energy ϵ is renormalized by a different factor Z' , which is also orbital dependent. Besides the band width renormalization, the orbital-selective correlation also leads to a redistribution of the electron density among the different orbitals, which is reflected by the renormalization of ϵ . In general, when the electron density n is increasing, the onsite energy decreases, and vice versa. In the 12-orbital model at $U = 0$, $\epsilon > 0$ for the $d_{xz/yz}$ orbitals,

and $\epsilon < 0$ for the d_{xy} orbital. We then expect the evolution of Z' to be in opposite to that of n in the $d_{xz/yz}$ orbitals whereas Z' follows the behavior of n in the d_{xy} orbital. This is indeed the case as shown in Fig. S3.

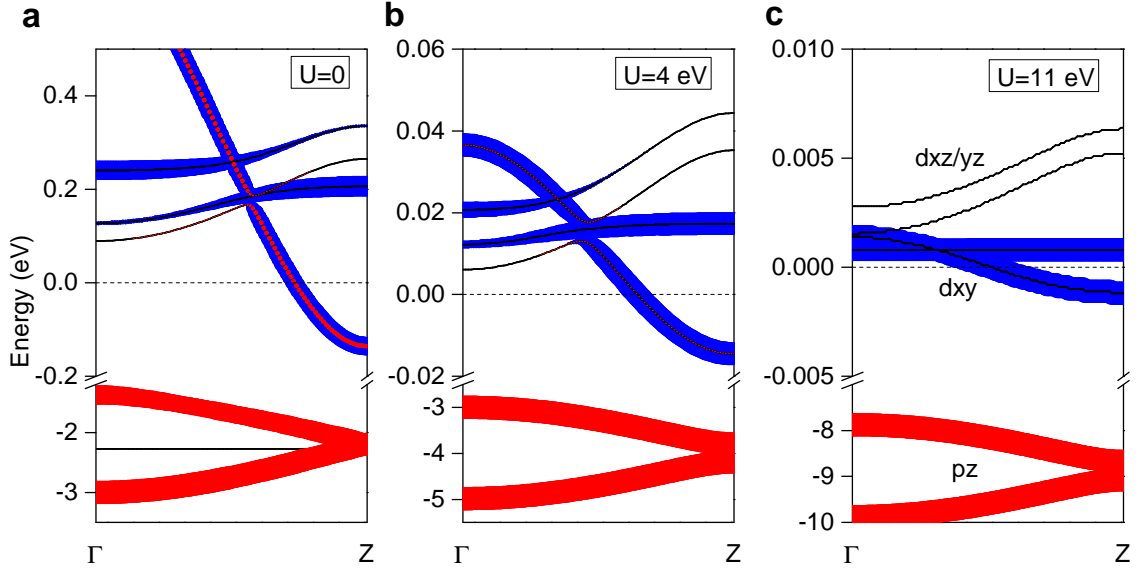


FIG. S4. (Color online) The band structures of the 12-orbital model for $\text{FeSe}_x\text{Te}_{1-x}$ at $x = 0.5$ along the Γ - Z direction of the BZ at $U = 0$ (a), for $U = 4$ eV (b), and for $U = 11$ eV (c), respectively. The thickness of the blue and red colors are proportional to the orbital weights of the d_{xy} and p_z orbitals, respectively.

As already mentioned, strong orbital-selective correlations significantly affect the band structure of the 12-orbital model. In Fig. S4, we show how the bandstructure along the Γ - Z direction evolves with increasing interaction U . With increasing U the major effects of the electron correlation on the bandstructure are as follows: First, the d orbital bands are strongly renormalized toward the Fermi energy E_F (set to 0 in the calculation). Second, the band inversion is a robust feature persisting up to $U \approx 10$ eV. Third, the hybridization between the d - and p -orbitals is weakened since this term is also renormalized by the factor of \sqrt{Z} of the associated d -orbital. Finally, as a consequence of the decoupling between the d - and p -orbitals and renormalization of the d -orbital bands, the p -orbital dominant bands are shifted to lower energies with increasing U .